Comparative Study of Turbulence Models in Predicting Turbulent Pipe Flow Part I: Algebraic Stress and k-ε Models

R. Martinuzzi* and A. Pollard†
Queen's University, Kingston, Ontario, Canada

A comparative study is presented of six different turbulence models simulating developing turbulent pipe flow. The models are a high and low Reynolds number version of the k-ε model; two versions of the algebraic stress models using the Naot et al.[12] prescription for the pressure-strain relationship, which differ in the prescription of the wall effect term; and two versions using the pressure-strain model proposed by Launder et al.[11] Tests were performed for a smooth circular pipe with a length-to-diameter ratio of 82.5 for bulk Reynolds numbers of 10,000, 38,000, 90,000, and 380,000. Predictions for the velocity, turbulence kinetic energy, and Reynolds stress field are compared to available experimental data. The relative performance of the models is assessed. It has been found that results obtained with the low Reynolds number k-ε model are in better agreement with experimental data than the results obtained from other models, especially at low Reynolds numbers.

Nomenclature

C_1, C_2, C_3 = constants in pressure-strain model
$C_{1\varepsilon}, C_{2\varepsilon}$ = constants in the modeled form of the ε transport equation
C_ε, C_k = constants in the algebraic stress model turbulence diffusion terms in k and ε equations
C_μ = constant in μ_t of k-ε model
D = pipe inner diameter
f_1, f_2 = function modifying $C_{1\varepsilon}$ and $C_{2\varepsilon}$ in ε equation
f_μ = function modifying C_μ in the k-ε models
k = turbulence kinetic energy
P = production term for k
P^* = mean hydrostatic pressure
P^{ij} = production term for Reynolds stresses
p = fluctuation component of hydrostatic pressure
R = pipe inner radius
Re = Reynolds number ($\equiv U_{\text{bulk}} D/\nu$)
R_k = turbulence Reynolds number ($\equiv k^{1/2} x_n/\nu$)
R_t = turbulence Reynolds number ($\equiv k^2/\varepsilon\nu$)
r = radial coordinate
T^{ij} = transport term for Reynolds stresses
U = axial mean velocity
U_{bulk} = average of axial mean velocity
U^+ = normalized velocity ($\equiv U/u_\tau$)
u_τ = friction velocity
V = radial mean velocity
x = axial coordinate
x_n = Cartesian coordinate normal to a solid surface
y = Cartesian coordinate normal to axial direction
y^+ = normalized wall coordinate ($\equiv y u_\tau/\nu$)
γ = constant in pressure-strain model
δ = height normal to surface of grid point directly adjacent to wall
δ_v = local height of viscous sublayer
δ^+ = ($\delta_v u_\tau/\nu$)
ε = homogeneous turbulence dissipation rate of k
ε^{ij} = turbulence dissipation rate of $\overline{u^i u^j}$
κ = von Karman's constant
λ = friction factor $\left[\equiv -\left(\frac{4D}{\rho U_{\text{bulk}}^2}\right) \Big/ \left(\frac{dP^*}{dx}\right) \right]$
μ = dynamic viscosity
μ_t = turbulence eddy viscosity
ν = kinematic viscosity
ρ = density
$-\rho\overline{u^i u^j}$ = Reynolds stress tensor
$-\rho\overline{u^2}$ = axial Reynolds normal stress
$-\rho\overline{uv}$ = Reynolds shear stress
$-\rho\overline{v^2}$ = radial Reynolds normal stress
$-\rho\overline{w^2}$ = tangential Reynolds normal stress
$\sigma_k, \sigma_\varepsilon$ = turbulence Prandtl-Schmidt numbers
τ_w = wall shear stress
τ^{ij} = shear stress tensor
Φ^{ij} = pressure-strain term
Ψ, ψ = general variables (scalar or vector)

Introduction

THE mathematical models employed in computational fluid dynamics codes often evolve from those developed for simpler flows. Indeed, some of the less complicated but usually well-understood and so-called benchmark flows are used as a source for the evaluation of the constants appearing in these models. The models are then tacitly presumed to be able to reproduce other flow cases of comparable complexity with equivalent success. A case in point is turbulent pipe flow. Most models of turbulence have been tested and/or developed using fully developed pipe flow conditions.[1,2] Although this case tends to be well reproduced, reports of developing pipe flow simulations are scarce and often incomplete;[3] that is, in contrast to other two-dimensional flows,[4,5] there apparently exists no concerted effort to fully and comprehensively document efforts to simulate developing turbulent pipe flow.

This apparent shortcoming has led the present authors to consider developing pipe flow as a predictive test case; that is, the authors posed the following question. Given a number of models of turbulence, implemented in the same computer code, using equivalent boundary conditions, solution methods, dis-

Received Sept. 19, 1986; revision received Dec. 28, 1987.

*Currently at Lehrstuhl für Strömungsmechanik, Universität Erlangen-Nürnberg, FRG.
†Associate Professor, Department of Mechanical Engineering.

cretization schemes, etc., how well can the developing turbulent flow in a pipe be predicted?

The models chosen for Part I of this study include the k-ε model in its high and low Reynolds number forms and four variants of an algebraic stress model (ASM).

The k-ε model used[6,7] is only applicable in fully turbulent regions of high Reynolds number flows and, thus, empirical wall-functions (which presume the existence of near-wall equilibrium flow) must be used to bridge the gap between the wall and core regions. The Lam and Bremhorst[1] low Reynolds number version of this model, which eliminates the need for wall-functions, is employed. This choice is based on the recommendations of Patel et al.[5]

The k-ε model of turbulence is considered to be the best among those in the two-equation model family, except in regions with adverse pressure gradients,[8] significant streamline curvature, and high shear.[9] It was proposed that the model fails because in weak shear conditions momentum diffusion is not adequately modeled by a Boussinesq gradient-driven mechanism, whereas in high-shear conditions the eddy viscosity is assumed isotropic, which is not verified experimentally.

The other four models used in this study are variants of an algebraic stress model obtained by algebraically modeling the net transport term T^{ij} in the Reynolds stress transport equation as proposed by Rodi.[10] By using the pressure-strain term representations developed by either Launder et al.[11] (hereafter referred to as LRR75) or Naot et al.[12] (hereafter referred to as NSW70), two forms of the ASM are obtained that use wall functions to link the near-wall flow to that in the core region. Two additional forms of the ASM are obtained by including a near-wall term that models the effects of the wall on the surrounding fluid.

In the present contribution, numerical tests have been performed at four Reynolds numbers for a pipe of length greater than 80 diam. The equations governing two-dimensional flow in cylindrical-polar coordinates are solved using control-volume-based finite-difference techniques that encompass higher order differencing and efficient pressure-velocity solution algorithms. The calculations presume that the flow is everywhere fully elliptic so that no biasing of the solution is introduced into the simulations, as is the case when the flow is presumed parabolic. Of course, this is of particular relevance in the inlet region of the pipe.

Models of Turbulence

The six models compared in this study are in a form valid for incompressible Newtonian fluids and are presented in generalized tensor notation (using the Einstein convention). The models are listed in Table 1. However, for convenience, some relevant features of the models are reviewed below.

The transport equation for the turbulence kinetic energy k and dissipation rate ε are of a similar form for all the models considered, but the algebraic expressions for the Reynolds stresses differ significantly.

The production term $P = -\overline{u^i u^k} U_{i,k}$ is determined by direct evaluation of the velocity field derivatives and the Reynolds stress field. The dissipation rate is obtained by solving the associated transport equation.

The turbulence diffusion term for both k and ε is modeled as for the k-ε models,

$$\text{Diff}(\psi) = \left(\nu + \frac{\nu_T}{\sigma_\psi}\psi_{,\ell}\right),_\ell \tag{1}$$

with $\sigma_k = 1$, as proposed by Harlow and Welch,[6] and $\sigma_\varepsilon = 1.3$ from Launder and Spalding.[7] For the ASM, the diffusion term can be expressed as[13]

$$\text{Diff}(\psi) = \left\{\nu\psi_{,\ell} + \left[\left(c_\psi f_\mu \frac{k}{\varepsilon}\right)\overline{u^k u^\ell}\right]\psi_{,k}\right\},_\ell \tag{2}$$

where $c_k = 0.22$ from Yang et al.[3] and $c_\varepsilon = 0.15$ from LRR75.

When determining the Reynolds stresses using the ASM, it is convenient to rewrite the relevant equation in the form

$$T^{ij} = P^{ij} - \varepsilon^{ij} + \Phi^{ij} \tag{3}$$

where

$$T^{ij} = D(\overline{u^i u^j})/Dt - \text{Diff}(\overline{u^i u^j})$$

and

$$\begin{aligned}
\text{Diff}(\overline{u^i u^j}) &= \{\nu(\overline{u^i u^j})_{,k} - (\overline{u^i u^j u^k}) - [\overline{p(u^i\delta^{jk} + u^j\delta^{ik})/\rho}]\},_k \\
\varepsilon^{ij} &= 2\nu\overline{u^i{}_{,k} u^j{}_{,k}} \\
\Phi^{ij} &= [\overline{p(u^{i,j} + u^{j,i})/\rho}] \\
P^{ij} &= -\overline{u^i u^k} U^j{}_{,k} - \overline{u^j u^k} U^i{}_{,k}
\end{aligned} \tag{4}$$

The transport term T^{ij} is[4]

$$T^{ij} = (P - \varepsilon/k)\,\overline{u^i u^j} \tag{5}$$

thereby allowing the Reynolds stress expressions to be completely algebraic. This operation reduces the numerical effort necessary in computing these stresses.

The production term P^{ij} is evaluated directly, but the dissipation rate ε^{ij} is modeled, assuming that the flow is locally isotropic,

$$\varepsilon^{ij} = \tfrac{2}{3}\varepsilon\delta^{ij} \tag{6}$$

The pressure strain term Φ^{ij} describes the mechanism by which interaction between the fluctuating pressure and the fluctuating velocity fields serve to redistribute the Reynolds stresses. The term is divided into a contribution due to the distortion of the Reynolds stress field Φ_1^{ij}, a contribution due to the distortion of the mean velocity field Φ_2^{ij}, and a term that arises due to the proximity of a solid boundary Φ_w^{ij}.

An explicit expression for the pressure-strain term can be obtained following Chou.[14] The term Φ_1^{ij} is approximated using Rotta's proposal[15] (see Table 1), where the coefficient C_1 is assumed constant. There appears to be disagreement over this coefficient. Lumley[16] showed that this coefficient should actually be interpreted as a tensor, with anisotropic elements of the form C^{ij}. Weinstock and Burk,[17] while substantiating these findings, indicate that, over a large range of Reynolds numbers and conditions, C^{ij} is independent of direction and invariant. It is, therefore, argued that this coefficient may be satisfactorily represented as a constant C_1 of value 1.5, according to LRR75.

The second term, Φ_2^{ij}, which arises due to distortion of the mean field, is modeled differently by NSW70 and LRR75. The latter group proposes a linear combination of Reynolds stresses that satisfies the physical and kinematic constraints.[15] The final form is

$$\Phi_2^{ij} = -B_1(P^{ij} - \tfrac{2}{3}P\delta^{ij}) - B_2 k(U^{i,j} + U^{j,i}) - B_3(D^{ij} - \tfrac{2}{3}P\delta^{ij}) \tag{7}$$

where

$$D^{ij} = -\overline{u^i u^k} U_k{}^{,j} - \overline{u^j u^k} U_k{}^{,i}$$

It was determined by NSW70 that under most circumstances the first term dominates all others and one may satisfactorily model Φ_2^{ij} by this term alone. Accordingly,

$$\Phi_2^{ij} = \gamma(P^{ij} - \tfrac{2}{3}P\delta^{ij}) \tag{8}$$

The constants C_1, B_1, B_2, B_3, and γ are obtained by reducing the transport equations for the case of homogeneous shear flow and comparing the results to those experimental data:[18] ($\overline{u^2}$/

$k-\frac{2}{3}) \approx 0.30$, $(\overline{v^2}/k-\frac{2}{3}) \approx -0.18$, and $(\overline{w^2}/k-\frac{2}{3}) \approx -0.12$. The local effect of a rigid solid wall on a fluid is expressed through Φ_w^{ij}. LRR75 give

$$\Phi_w^{ij} = \left[c_3\left(\frac{\varepsilon}{k}\right)\left(\overline{u^iu^j} - \frac{2}{3}k\delta^{ij}\right) + c_4\left(P^{ij} - D^{ij}\right)\right]\frac{k^{3/2}}{\varepsilon x_n} \quad (9)$$

where x_n is the distance normal to the wall; c_3 and c_4 are obtained from a consensus[11,19] for near-wall values: $(\overline{u^2}/k)-\frac{2}{3} \approx 0.51$, $(\overline{v^2}/k)-\frac{2}{3} \approx -0.42$, and $(\overline{w^2}/k)-\frac{2}{3} \approx -0.09$.

Thus, two k-ε models and four ASM can be constructed from the various components outlined (see Table 1).

Numerical Procedure

The flow under consideration is presumed two-dimensional. The common practice of using the parabolic forms of the governing equations (that is, setting all second-order longitudinal gradients to zero) was deemed inappropriate. Hence, the equations were solved in their full elliptic forms.

The equations were discretized using finite-volume techniques and the hybrid differencing scheme (HDS).[20] Tests were also performed using the QUICKER[21] version of the QUICK scheme.[22] The results in the wall region and in the entrance region differed slightly from those results obtained using HDS, but the difference, in the authors' opinion, was not large enough to warrant the extra computational effort required by the higher-order QUICKER scheme.

The SIMPLE solution algorithm[23] was used to effect a solution to the momentum and continuity equations. However, this algorithm is not necessarily the most efficient method, as shown by, for example, Latimer and Pollard.[24] Thus, CTS-SIMPLE[25] and SIMPLEC[26] were also used. SIMPLEC is used for k-ε models and CTS-SIMPLE for the ASM models.

The problem was solved using 120 to 180 points in the axial direction and 40 to 66 points in the radial direction. Both uniform and nonuniform staggered grids were used.

Boundary Conditions

The simulations were performed using equivalent conditions for all models. A uniform profile is assumed for all quantities at the pipe inlet: the axial velocity is assigned the bulk value and the radial velocity is assumed zero. The values of the Reynolds stresses are also stored and evaluated directly at the grid points using algebraic relations and, therefore, boundary conditions are not strictly required as these would overspecify the problem.

Empirical relationships are used to assign entrance values to k and ε; that is, $k = 0.005U_{\text{bulk}}^2$ and $\varepsilon = (C_\mu k^{\frac{3}{2}}/0.03R)$.

The pipe section was chosen to be sufficiently long so that fully developed conditions could be assumed to prevail at the outlet; that is, all axial derivatives were assumed negligible. At the pipe axis, symmetry is assumed: $(\partial\phi/\partial r) = V = 0$, where ϕ can be any of U, k, or ε.

To satisfy the no-slip condition at the wall when the grid point adjacent to the wall was located outside the viscous sublayer ($y^+ \geqslant 11.63$), the wall shear stress was everywhere evaluated assuming the existence of a log-law.

For the turbulence qualities, the boundary conditions cannot be applied directly at the pipe wall (except for the low

Table 1 Summary of turbulence models

Common equations: k: $(Dk/Dt) = \text{Diff}(k) + P - \varepsilon$; ε: $(D\varepsilon/Dt) = \text{Diff}(\varepsilon) + (\varepsilon/k)(c_{1\varepsilon}f_1P - c_{2\varepsilon}f_2\varepsilon)$

Constants: $c_{1\varepsilon} = 1.44$, $c_{2\varepsilon} = 1.92$

M	Name	$\rho\overline{uv}$	Diff(Ψ)	Φ_w^{ij}	Φ_2^{ij}
1	High Re k-ε	$\frac{2}{3}\rho k\delta^{ij} - \mu_t(U^{i,j} + U^{j,i})$	$\left[\left(\nu + \frac{\nu_t}{\sigma_\Psi}\right)\Psi_{,\ell}\right]_{,\ell}$	N/A	N/A
2	Low Re k-ε	$\mu_t = \rho C_\mu f_\mu (k^2/\varepsilon)$	$\sigma_k = 1$ $\sigma_\varepsilon = 1.3$		
3	Naot et al.[12] no wall-term	$\dfrac{\rho k}{(c_1-1)\varepsilon + P}^*$	$(\nu\Psi_{,\ell} + [c_\Psi(k/\varepsilon)]\overline{u^iu^\ell}]_{\Psi,i})_{,\ell}$	Zero	$\gamma(P^{ij} - \frac{2}{3}P\delta^{ij})$
4	Naot et al.[12] with wall term	$\{P^{ij} - \varepsilon^{ij} + \Phi_1^{ij} + \Phi_2^{ij} + \Phi_w^{ij}\}$	$\Psi = k$ or ε $\varepsilon^{ij} = \frac{2}{3}\varepsilon\delta^{ij}$	f_ℓ	$\gamma = 0.6$
5	Launder et al.[11] no wall term	$c_1 = 1.5$ $c_3 = 0.015$ $c_4 = 0.125$	$c_k = 0.22$ $c_\varepsilon = 0.15$	Zero	$-B_1(P^{ij} - \frac{2}{3}P\delta^{ij})$ $-B_2k(U^{i,j} + U^{j,i})$ $-B_3(D^{ij} - \frac{2}{3}P\delta^{ij})$
6	Launder et al.[11] with wall term			f_ℓ	$B_1 = 0.764$ $B_2 = 0.182$ $B_3 = 0.109$

$\Phi_1^{ij} = c_1(\varepsilon/k)(\overline{u^iu^j} - \frac{2}{3}k\delta^{ij})$

$M = 1$: $C_\mu = 0.09$; $f_1 = f_2 = f_\mu = 1$

$M = 2$: $C_\mu = 0.09$; $f_\mu = [1 - \exp(-A_\mu R_k)]^2[1 + (A_t/R_t)]$; $f_1 = 1 + [A_{c1}/f_\mu]^3$; $f_2 = 1 - \exp(-R_t^2)$; $A_\mu = 0.0165$, $A_t = 20.5$, $A_{c1} = 0.05$

$M = 4,6$: $f_\ell = \{c_3(\epsilon/k)(\overline{u^iu^j} - \frac{2}{3}k\delta^{ij}) + c_4(P^{ij} - D^{ij})\}(k^2/\epsilon x_n)$

Reynolds number k-ε model) because these models are all developed assuming a fully turbulent regime. This condition is not satisfied close to the wall; consequently, it is necessary to prescribe profiles in the region spanning the wall and the fully turbulent region.

The near-wall flow domain is assumed to consist of two regions[27]: a viscous sublayer extending to $y^+ \approx 11.63$ and a fully turbulent region extending out into the core region. If the grid point adjacent to the wall is in the viscous sublayer, it is necessary to specify the shear stresses, since the ASM cannot be applied directly in this region. Thus, the values of $\overline{u^i u^j}$ and the boundary conditions for k are obtained by applying continuity close to the wall:[5]

$$k = k_v(y^+/\delta^+)^2$$

$$\overline{u^2} = u_v(y^+/\delta^+)^2$$

$$\overline{v^2} = v_v(y^+/\delta^+)^4$$

$$\overline{w^2} = w_v(y^+/\delta^+)^2$$

$$\overline{uv} = d_v(y^+/\delta^+)^3$$

where δ^+ is the local thickness of the viscous sublayer. The values of the k_v, u_v, v_v, w_v, and d_v are obtained by linearly extrapolating the values of the related variable in the outer-flow to the edge of the viscous sublayer. However, it has been found[19] that the $\overline{uv}$ field can be better represented by

$$\overline{uv} \cong \begin{cases} 0.008(y^+)^3 & \text{for } y^+ \leq 5 \\ d_v \dfrac{y^+ - 5}{11.63} + 0.1U_r^2 & 5 \leqslant y^+ \leqslant 11.63 \end{cases} \tag{10}$$

The boundary condition for ε is obtained by reducing the transport equation for k for near-wall flow such that

$$\varepsilon_{\text{wall}} = \nu \left.\frac{\partial^2 k}{\partial x_n^2}\right|_{\text{wall}} \tag{11}$$

If the grid point next to the wall is assumed to be in the fully turbulent region, the following empirical boundary conditions, which hold between about $60 \leqslant y^+ \leqslant 150$ but are still approximately valid to the edge of the viscous sublayer,[5] are implemented:

$$\frac{\partial k}{\partial x_n} = \frac{\partial \varepsilon}{\partial x_n} = 0 \tag{12}$$

together with the empirical wall functions

$$\varepsilon_{\text{wall}-1} = (C_\mu k^2/\kappa x_n) \tag{13}$$

As noted previously, boundary conditions for the Reynolds stresses are not necessary when the last grid point is in the fully turbulent region.

For the low Reynolds number k-ε model, which is applicable even in the viscous sublayer, the physical boundary conditions for k and ε are directly implemented; that is,

$$k_{\text{wall}} = \left.\frac{\partial k}{\partial x_n}\right|_{\text{wall}} = 0 \tag{14}$$

and Eq. (11).

Presentation and Discussion of Results

The numerical calculations were performed on an IBM 3081G mainframe computer. The results were determined to be independent of the grid size within 5%, using the h^m extrapolation technique[28] on randomly chosen points in the flow domain. The grid specifications used and the solution-convergence times are summarized in Table 2. Note that, at higher Reynolds numbers, a finer grid was used in order to achieve the necessary resolution in the high-gradient, near-wall region that is, for this flow, characteristically thinner than at lower Reynolds numbers.

The distributions of U, V, $\overline{u^2}$, $\overline{v^2}$, $\overline{w^2}$, $\overline{uv}$, k, ε, τ_w, and λ (defined in the nomenclature) have been obtained for each of the 24 cases (6 models each at Re = 10,000, 38,000, 90,000, and 380,000). The calculated results are compared to one another, and, for the sake of placing the calculations in perspective, they are compared to various data sets that appear in the literature. A single data set has not been used because, in the authors' opinion, a reliable, well-documented data set does not exist; that is, one that has not provided well-documented inlet conditions.[29] As a result, the calculations to be presented are discussed in light of this obvious deficiency. The data sets used in this part of the paper are those of Richman and Azad,[30] Lawn,[31] Barbin and Jones,[32] and Nikuradse.[33] The results at

Table 2 Grid selection and CPU time

Case	Re	Model	Grid	CPU, min	Comments
		1	120 × 40	22	—
		2	120 × 66	313	54% of pts. $\leqslant y^+ = 40$
1	10,000	3,5	120 × 40	213	High residuals; poor convergence
		4	120 × 40	218	High residuals; conv. difficult to obtain
		6	120 × 30	> 220	Convergence criterion not met
		1	120 × 50	48	—
		2	120 × 66	318	30% of pts. $\leqslant y^+ = 40$
2	38,000	3,5	120 × 50	231	High ε residuals
		4,6	120 × 50	240	—
		1	120 × 60	52	—
	90,000	2	120 × 66	457	22% of pts. $\leqslant y^+ = 40$
3,4	380,000	3,5	120 × 50	284	—
		4,6	120 × 50	290	—

$M = 1$ High Re k-ε model of Launder and Spalding.[7]
$M = 2$ Low Re k-ε model of Lam and Bremhorst (1978, 1981).[1]
$M = 3,4$ ASM of Naot et al.[12] with and without Φ_w^{ij}.
$M = 5,6$ ASM of Launder et al.[11] with and without Φ_w^{ij}.

$Re = 90{,}000$ and 380,000 are very similar, and the trends at $Re = 38{,}000$ are the same as those found for $Re = 10{,}000$, except that the features of the latter are more dominant than those of the former. Thus, only those results for $Re = 10{,}000$ and 380,000 are shown. The detailed results can be found elsewhere.[19]

In Fig. 1, the fully developed axial velocity profiles, at $Re = 380{,}000$, are compared; also plotted are those data of Nikuradse.[33] The calculations compare well. Of course, this is to be expected, as the models were developed assuming fully turbulent flow conditions.

The fully developed profiles at $Re = 380{,}000$ are shown plotted in the form u^+ vs y^+ in Fig. 2. The slopes are generally well reproduced, but the absolute values of the calculations tend to underpredict the data of Nikuradse.[33] The u^+intercept, in the case of the Lam and Bremhorst[1] k-ε model ($M = 2$), is slightly low implying that the calculated τ_w is high. The value of the intercept B is very sensitive to the value of the von Karman's constant κ. For example, with $\kappa = 0.4$, B is 5.5, and with $\kappa = 0.41$, B is 4.9. Since both values for B are quoted in the literature (see, for example, Schlichting[34]), it is believed this difference is of little consequence.

The developing axial velocity, as a function of inlet distance, of little consequence is shown in Fig. 3. Except in the core region, $r/R = 0$, the numerical results reproduce well the experimental ones, and the results from different models are virtually indistinguishable. For the centerline velocity, the calculations agree well with the data of Barbin and Jones[32] in the inlet region but drop off gradually to approach values given by Nikuradse[33] (which are not shown for clarity) for fully developed flow.

The developing velocity profiles for $Re = 380{,}000$ are shown in Fig. 4 with the data of Barbin and Jones.[32] Again, the differences are negligible. The results shown in Figs. 1-4 satisfy the requirement that at least fully developed, fully turbulent pipe-flow at high Reynolds numbers can be adequately simulated.

The models have been developed with the assumption that the flow is locally isotropic. It is natural to ask how the performance of the models is affected by conditions that are increasingly removed from those of local isotropy, as is the case, for example, at lower Reynolds numbers.

In Fig. 5, the fully developed axial velocity profiles, at $Re = 10{,}000$, are compared with those data of Nikuradse.[33] Note that, with the exception of the low Re k-ε model,[1] the agreement between experimental data and simulations is poorer than at higher Reynolds numbers. Furthermore, as seen when plotting the profiles in the form u^+ vs y^+, as in Fig. 6, the log-law region is generally poorly reproduced by the ASM; that is, both slope and intercept are incorrect. Possible reasons for these discrepancies will be addressed shortly.

The radial distributions of the $\overline{uv}$ field are shown for a Reynolds number of 380,000 in Figs. 7 and 8. Note that because of space restrictions, the fully developed profiles are not shown. Suffice it to say, a linear distribution is obtained that is in excellent agreement with experimental data. Results obtained using different versions of the ASM almost coincide, indicating that for these distributions the effect due to the alternate prescriptions for Φ_2^{ij} and Φ_w^{ij} is negligible. At $x/D \approx 10$, the ASM predictions agree well with the data of Richman and Azad[30] implying that the flow, for modeling purposes, indeed can be treated as behaving as locally isotropic; a point of crucial importance when modeling the transport T^{ij} and dissipation ε^{ij} terms. In formulating the model for T^{ij}, it is required that the ratios $(\overline{u^i u^j}/k)$ be nearly constant or slowly changing, a condition most readily satisfied in isotropic flow. A possible shortcoming of the modeling of the Reynolds stresses in the k-ε model is suggested by the consistent underprediction of the $\overline{uv}$ field at this Reynolds number.

Between x/D of 30 and 40 from the inlet, the predicted values for the turbulence shear stresses are greater than those in the fully developed region (see Fig. 8). This behavior may be explained as follows. As shown in Fig. 6, the centerline axial

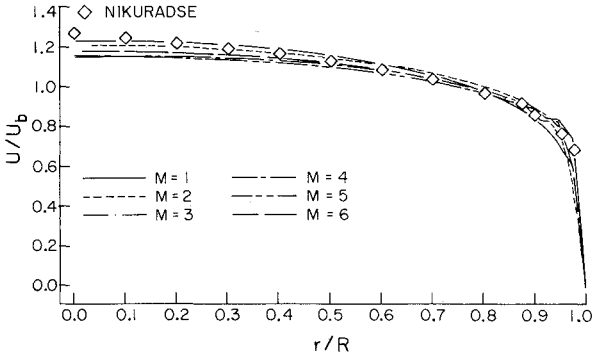

Fig. 1 Axial velocity vs r/R at $x/D = 80$ for $Re = 380{,}000$.

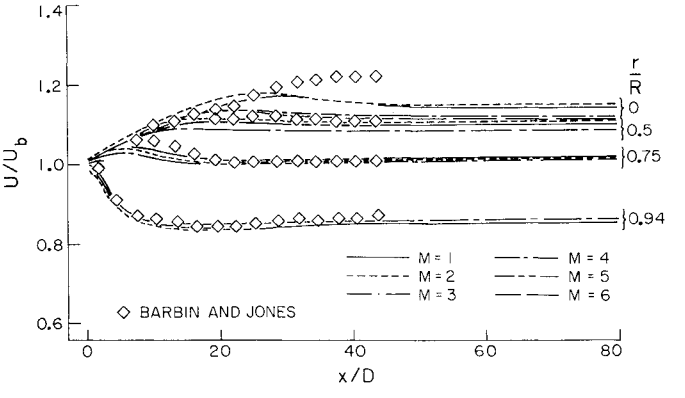

Fig. 3 Variation of axial velocity with distance downstream of pipe inlet for $r/R = 0$, 0.5, 0.75, 0.94 for $Re = 380{,}000$.

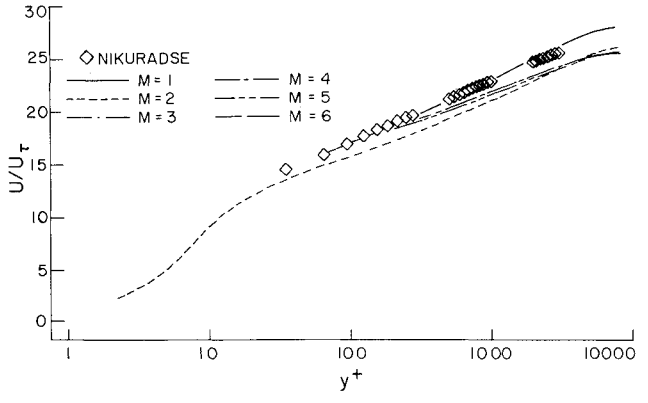

Fig. 2 u^+ vs y^+ at $x/D = 80$ for $Re = 380{,}000$.

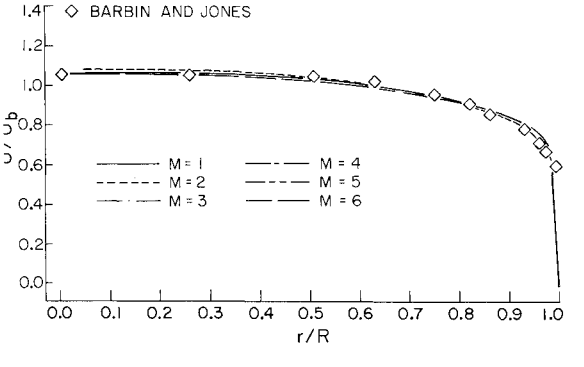

Fig. 4 Axial velocity vs r/R at $x/D = 16$ for $Re = 380{,}000$.

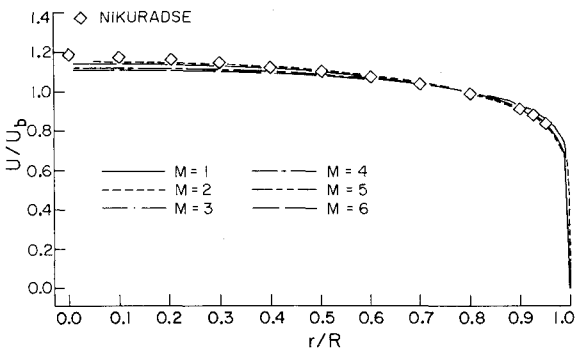

Fig. 5 Axial velocity vs r/R at $x/D = 80$ for $Re = 10{,}000$.

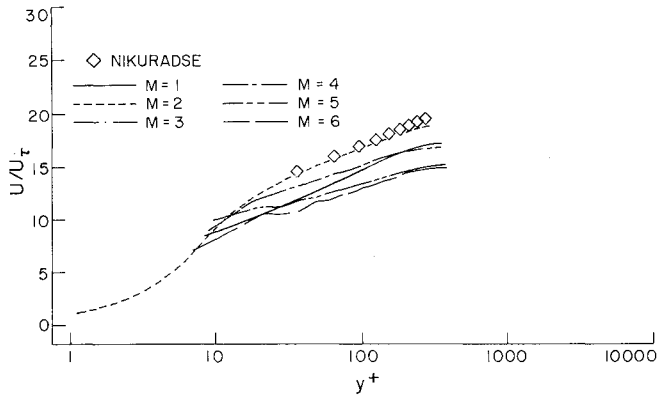

Fig. 6 u^+ vs y^+ at $x/D = 80$ for $Re = 10{,}000$.

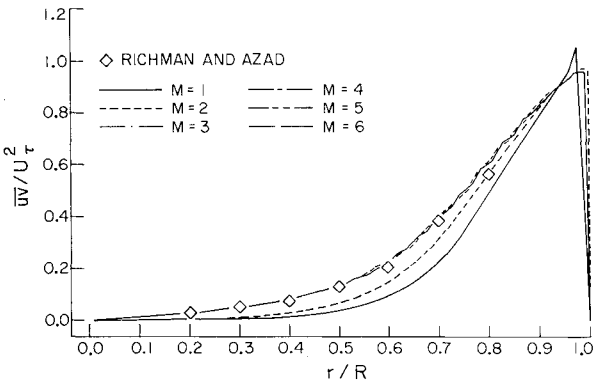

Fig. 7 Reynolds shear stress vs r/R at $x/D = 10$ for $Re = 380{,}000$.

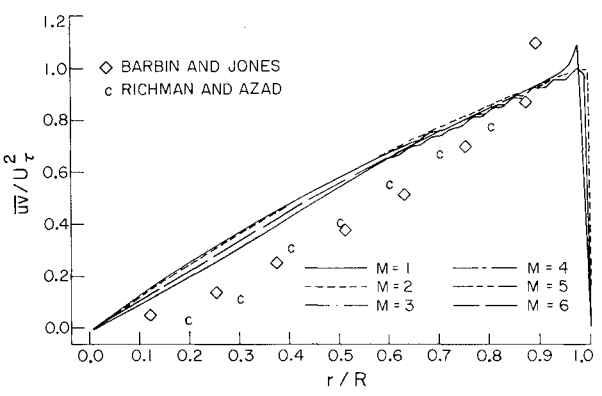

Fig. 8 Reynolds shear stress vs r/R at $x/D = 29$ for Re 380,000.

velocity increases until it reaches a maximum at $x/D \approx 20$, then decreases between $x/D \approx 30$ and 40, which, in accordance with the principle of conservation of mass, requires fluid to be convected towards the pipe wall. The velocity gradients are, consequently, negative over most of the pipe cross section, resulting in an increase in the production of $\overline{uv}$. The reader is referred to Klein[29] for alternative interpretations. Even so, consistent as this argument may be, it is uncertain whether this additional production is sufficiently large to cause the numerically predicted behavior.

Previous simulations,[3] using the ASM as prescribed by NSW70 that includes the wall effect term ($M = 4$), agree well with the prescribed results. Unfortunately, the results for $\overline{uv}$ between $30 \leqslant x/D \leqslant 70$ were not made available, and there are no experimental data for the turbulence shear stress between $30 \leqslant x/D \leqslant 40$. It is, however, of interest to note that Barbin and Jones[32] also report values for $\rho\overline{uv}$ in excess of the local wall shear stress for x/D of about 29 and 41.

The profiles for $\overline{uv}$, at $x/D = 10$, for a Reynolds number of 10,000, are shown in Fig. 9. The k-ε model simulations predict a flow development that is in accord with those data of Richman and Azad.[30] In the ASM simulations, the development of the $\overline{uv}$ field is clearly too rapid; however, recall that the ASM, at this Reynolds number, underpredicted the fully developed profiles of axial velocity (Fig. 6). The jagged profile close to the wall is caused by an improper location of the $\overline{uv}$ nodes on the finite-difference grid. The values were stored at the grid points and not at the corners of the control volumes. However, for the calculation of other parameters, only the value between $\overline{uv}$ nodes was necessary, so that the behavior observed here has no effect on any other result.

The fully developed $\overline{uv}$ profile is shown in Fig. 10. Observe that the low Reynolds number effects in the Lam and Bremhorst[1] k-ε model ($M = 2$) cause a rapid damping of $\overline{uv}$ close to the wall, which is more pronounced than for the high Reynolds number version of this model ($M = 1$).

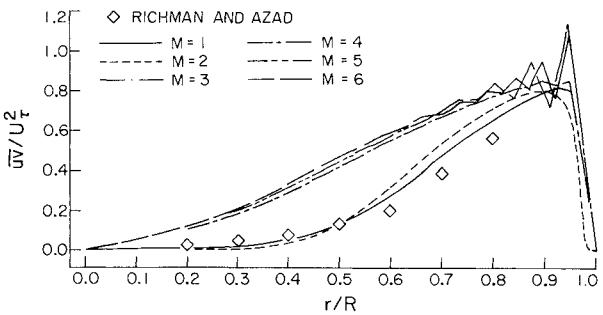

Fig. 9 Reynolds shear stress vs r/R at $x/D = 10$ for $Re = 10{,}000$.

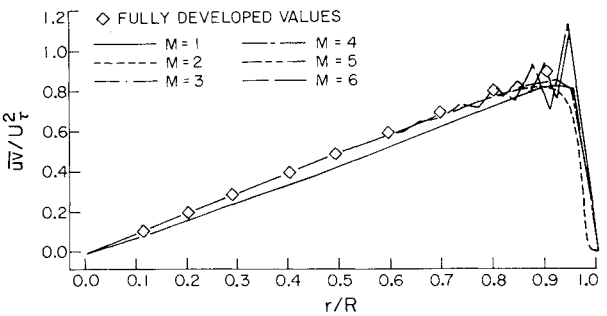

Fig. 10 Reynolds shear stress vs r/R at $x/D = 80$ for $Re = 10{,}000$.

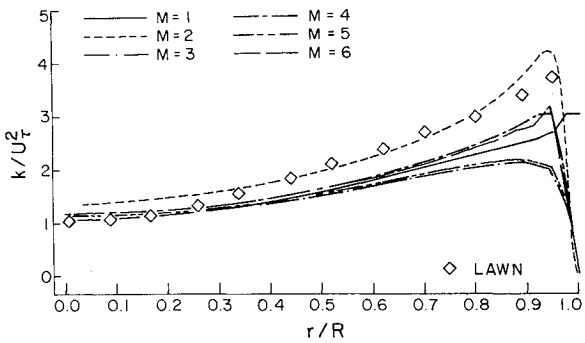

Fig. 11 Turbulence kinetic energy vs r/R at $x/D = 80$ for $Re = 10{,}000$.

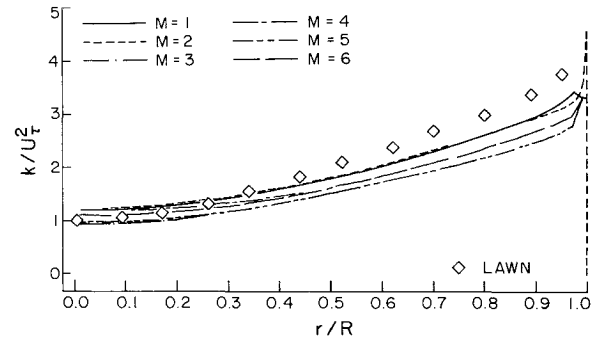

Fig. 12 Turbulence kinetic energy vs r/R at $x/D = 80$ for $Re = 380{,}000$.

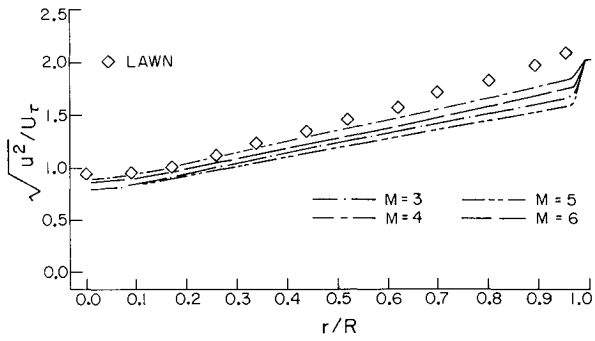

Fig. 13 Axial Reynolds normal stress vs r/R at $x/D = 80$ for $Re = 380{,}000$.

The distribution of the turbulence kinetic energy in the fully developed region for Reynolds numbers of 10,000 and 380,000 is shown in Figs. 11 and 12, respectively. The low Reynolds number version of the k-ε model ($M = 2$) predicts the experimental data of Lawn[31] quite well. The high Reynolds number k-ε model simulations differ from the low Reynolds version only at 10,000, thereby indicating the importance of low Reynolds number effects. The ASM predictions fall on two curves, one for models that include the wall effect term ($M = 4,6$) and the other for models that do not include this term ($M = 3,5$). Observe that the near-wall predictions are least adequate indicating a possible inappropriate modeling of Diff (k) in regions of high shear (or low Re_k). That is, in the ASM, it can be argued that the pressure strain term should not affect the transport of k, since $\Phi^{ii} = 0$, although this term does have an effect on the distribution of k through the normal and shear stress terms that appear in the k production and diffusion terms.

The approximation used in formulating T^{ij} is best in the core region and at high Reynolds numbers. As the Reynolds number drops or as the mean flow gradients become too large (see Figs. 11–14), this approximation gradually becomes less adequate.

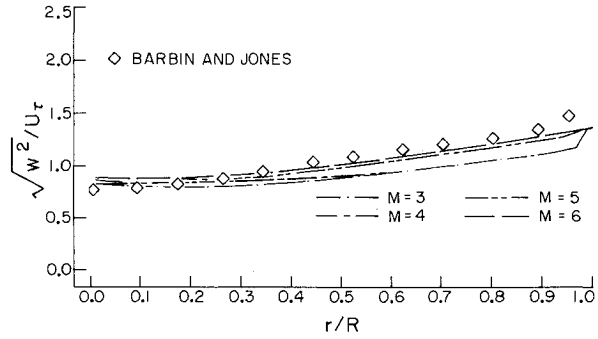

Fig. 14 Tangential Reynolds normal stress vs r/R at $x/D = 80$ for $Re = 380{,}000$.

The effect of the redistribution term D^{ij}, found in the Φ_2^{ij} term as proposed by LRR75, can be seen in Figs. 13 and 14, which show the u_{rms}/U_τ and w_{rms}/U_τ in the fully developed region at a Reynolds number of 380,000.

Generally, the models containing the D^{ij} term ($M = 5,6$) tend to give a lower estimate for $\overline{u^2}$ and higher estimates for $\overline{w^2}$ than do those of NSW70 ($M = 3,4$). The D^{ij} term can be interpreted as providing a mechanism for the transfer of energy between Reynolds stress fields (as observed by, for example, Barbin and Jones[32]). Consider the transport equation for $\overline{u^2}$ as proposed by NSW70. It is clear that the Reynolds stresses appear explicitly in the production term P^{xx}. In this term, $\overline{u^2}$ is only affected by the U field and by the shear stresses $\overline{uv}$ and $\overline{uw}$. The U field is, in turn, only directly affected by $\overline{u^2}$, $\overline{uv}$, and $\overline{uw}$ in the U momentum equation. Consequently, the $\overline{u^2}$ field is coupled to the v^2 and w^2 fields only through the shear stress field, which is a very weak link, and the fields could be treated, in this context, as being uncoupled. If the D^{xx} term is introduced into the $\overline{u^2}$ transport equation, as is done by LRR75, the $\overline{u^2}$ field is now directly affected by the V and W fields, which are in turn directly affected by the $\overline{v^2}$ and $\overline{w^2}$ fields. This relationship between normal stress fields is more direct; it also provides the mechanism for the energy transfer between normal stress fields. A similar argument for the shear stress fields is difficult to construct because these fields are more strongly coupled and interlinked.

Conclusions and Recommendations

In this paper, the developing turbulent flow in a pipe has been calculated at four Reynolds numbers using six models of turbulence. While experimental data sufficient for quantitative assessment of the models are lacking in the literature, the trends observed in the calculated results permit the following conclusions to be drawn.

1) As might be expected, since the low-Reynolds number k-ε model was developed using fully developed pipe flow as a basis, it provides the best predictions. However, it has limited versatility and the costs of its implementation are comparable to those incurred using the more versatile ASM.

2) The ASM are restricted to relatively high Reynolds number flows, or to conditions where shear is not too severe, so that the assumptions made in formulating T^{ij} are still valid.

3) None of the ASM predict $\overline{u^2}$ and k particularly well, especially in the near-wall region. It has been suggested that this is because the wall effect term is not being adequately represented and because there is no modification of the k diffusion term to account for the effect of the wall proximity, as in the case in the k-ε model.

4) The D^{ij} term is necessary in Φ_2^{ij}, as it provides a mechanism for the energy transfer between normal stress fields; therefore, the LRR75 model is preferable to the NSW70 model.

5) Although its damping function appears inadequate, Φ_w^{ij} is necessary.

Based on these conclusions, the authors recommend that further work of this type be considered and undertaken, both experimentally and computationally, in order to provide a wide and firmly established data base for future developments. Attention should be focused on the behavior of the $\overline{uv}$ field in the entrance region and to documenting the whole flowfield properly, particularly in the entrance region and in the vicinity of a solid boundary.

Acknowledgments

This study was made possible by grants and graduate scholarships from the Natural Sciences and Engineering Research Council of Canada. The authors are also indebted to Queen's University for supplying unlimited computer time, without which this study could not have been undertaken. This paper was prepared while A. Pollard was an Alexander von Humboldt Fellow at Lehrstuhl für Strömungsmechanik.

References

[1]Lam, C. K. G. and Bremhorst, K., "A Modified Form of the k-ε Model for Predicting Wall Turbulence," *Journal of Fluids Engineering*, Vol. 103, 1981, pp. 456–460.

[2]So, R. M. C. and Yoo, G. J., "On the Modeling of Low-Reynolds-Number Turbulence," NASA Rept. 3994, 1986.

[3]Yang, C. I., Kao, T. T., Bartzis, J. G., and Sha, W. T., "Numerical Modeling of Turbulent Flow in Pipes with a Reynolds Stress Closure," ASME/ASCE Conference, Boulder, Colorado, 1981.

[4]Rodi, W., "Comparison of Computation with Experiment," *Proceedings, 1980–81, AFOSR-HTTM-Stanford Conference on Complex Turbulent Flows,* Vol. 2, edited by J. J. Kline, B. J. Cantwell, and G. M. Lilley, pp. 1495–1516.

[5]Patel, V. C., Rodi, W., and Scheuerer, G., "Evaluation of Turbulence Models for Near-Wall and Low-Reynolds Number Flows," *AIAA Journal*, Vol. 23, Sept. 1985, pp. 1308–1319.

[6]Harlow, F. H. and Welch, J. E., "Numerical Calculation of Time-Dependent Viscous Incompressible Flow of Fluid with a Free Surface," *Physics of Fluids*, Vol. 8, 1965, pp. 2182–2189.

[7]Launder, B. E. and Spalding, D. B., "The Numerical Computation of Turbulent Flows," *Computer Methods in Applied Mechanics and Engineering*, Vol. 3, 1974, pp. 269–289.

[8]Chambers, T. L. and Wilcox, D. C., "Critical Examination of Two-Equation Turbulence Closure Models for Boundary Layers," *AIAA Journal*, Vol. 15, June 1977, pp. 821–828.

[9]Pourahmadi, F. and Humphrey, J. A. C., "Prediction of Curved Channel Flow with an Extended k-ε Model of Turbulence," *AIAA Journal*, Vol. 21, Oct. 1983, pp. 1365–1373.

[10]Rodi, W., "The Prediction of Free Turbulent Boundary Layers by use of a Two-Equation Model of Turbulence," Ph.D. Thesis, Univ. of London, England, 1972.

[11]Launder, B. E., Reece, G. J., and Rodi, W., "Progress in Development of Reynolds-Stress Turbulence Model," *Journal of Fluid Mechanics*, Vol. 68, 1975, pp. 537–566.

[12]Naot, D., Shavit, A., and Wolfstein, M., "Interactions Between Components of the Turbulent Velocity Correlations Tensor," *Israel Journal of Technology*, Vol. 8, 1970, p. 259.

[13]Daly, B. J. and Harlow, F. H., "Transport Equations of Turbulence," *Physics of Fluids*, Vol. 13, 1970, pp. 2634–2649.

[14]Chou, P. Y., "On Velocity Correlations and the Solutions for the Equations of Turbulence," *Quarterly Journal of Applied Mathematics*, Vol. 3, No. 1, 1944, pp. 38–52.

[15]Rota, J., "Statistische Theorie Nichthomogener Turbulenz," Zeitschrift für Physik, Vol. 129, 1951, p. 547.

[16]Lumley, J. L., "Computational Modelling of Turbulent Flows," *Advances in Applied Mechanics*, Vol. 18, 1978, pp. 123.

[17]Weinstock, J. and Burk, S., "Theoretical Pressure-Strain Term, Experimental Comparison and Resistance to Large Anisotropy," *Journal of Fluid Mechanics*, Vol. 154, 1985, pp. 429–443.

[18]Champagne, F. H., Harris, V. G., and Corrisin, S., "Experiments on Nearly Homogeneous Shear Flows," *Journal of Fluid Mechanics*, Vol. 41, 1970, pp. 81–139.

[19]Martinuzzi, R., "Comparative Study of Turbulence Models in Simulating Developing Turbulent Pipe Flow," M.S. Thesis, Dept. of Mechanical Engineering, Queen's Univ., Kingston, Ontario, Canada, 1985.

[20]Spalding, D. B., "A Novel Finite-Difference Formulation for Differential Expressions Involving Both First and Second Derivatives," *International Journal of Numerical Methods in Engineering*, Vol. 4, 1972, pp. 551–559.

[21]Pollard, A. and Siu, A. L.-W., "The Calculation of Some Laminar Flows Using Various Discretisation Schemes," *Computer Methods in Applied Mechanics and Enginering*, Vol. 35, 1982, pp. 293–313.

[22]Leonard, B. P., "A Stable and Accurate Convective Modelling Procedure Based on Quadratic Upstream Interpolation," *Computer Methods in Applied Mechanics and Engineering,* Vol. 19, 1979, pp. 59–98.

[23]Patankar, S. V. and Spalding, D. B., "A Calculation Procedure for Heat, Mass and Momentum Transfer in Three-Dimensional Parabolic Flows," *International Journal of Heat and Mass Transfer*, Vol. 15, 1972, p. 1787.

[24]Latimer, B. R. and Pollard, A., "A Comparison of Pressure Velocity Coupling Solution Algorithms," *Numerical Heat Transfer*, Vol. 8, 1985, pp. 635–652.

[25]Raithby, G. D. and Schneider, G. E., "Numerical Solution of Problems in Incompressible Fluid Flow: Treatment for the Pressure-Velocity Coupling," *Numerical Heat Transfer*, Vol. 2, 1979, pp. 417–440.

[26]Van Doormal, J. P. and Raithby, G. D., "Enhancement of the SIMPLE Method for Predicting Incompressible Fluid Flows," *Numerical Heat Transfer*, Vol. 7, 1984, pp. 147–163.

[27]Johnson, R. W. and Launder, B. E., "Discussion of 'On the Calculation of Turbulent Heat Transport Downstream from an Abrupt Pipe Expansion,'" *Numerical Heat Transfer*, Vol. 5, 1982, pp. 493–496.

[28]Crandall, S. H., *Engineering Analysis*, Kruger Publishing, Malabar, FL, 1983.

[29]Klein, A., "REVIEW: Turbulent Developing Pipe Flow," *Journal of Fluids Engineering*, Vol. 103, 1981, pp. 242–249.

[30]Richman, J. W. and Azad, R. S., "Developing Turbulent Flow in a Smooth Pipe," *Apl. Sci. Res.*, Vol. 28, 1973, pp. 419–441.

[31]Lawn, C. J., "Rate of Dissipation in Turbulent Pipe Flow," *Journal of Fluid Mechanics*, Vol. 48, 1971, pp. 477–505.

[32]Barbin, A. J. and Jones, J. B., "Turbulent Flow in the Inlet Region of a Smooth Pipe," *ASME Journal of Basic Engineering*, Vol. 29, 1963, pp. 29–34.

[33]Nikuradse, J., "Gesetzmä β ig keit der turbulenten Strömung in glatten Rohren," Verein Deutscher Ingenieure-Forschungsheft, No. 356, 1932.

[34]Schlichting, H., *Boundary-Layer Theory*, McGraw-Hill, New York, 1968.